Fluid transport in nanochannels induced by temperature gradients

Chong Liu, Ya Lv, and Zhigang Li

Additional information on J. Chem. Phys.

Fluid transport in nanochannels induced by temperature gradients

Chong Liu,[1,2] Ya Lv,[1] and Zhigang Li[1,a]

[1]*Department of Mechanical Engineering, The Hong Kong University of Science and Technology, Clear Water Bay, Kowloon, Hong Kong*
[2]*Laboratory of High Temperature Gas Dynamics, Institute of Mechanics, Chinese Academy of Sciences, Beijing, People's Republic of China*

We investigate the mechanisms of fluid transport driven by temperature gradients in nanochannels through molecular dynamics simulations. It is found that the fluid-wall interaction is critical in determining the flow direction. In channels of very low surface energy, where the fluid-wall binding energy ε_{fw} is small, the fluid moves from high to low temperature and the flow is induced by a potential ratchet near the wall. In high surface energy channels, however, the fluid is pumped from low to high temperature and the pressure drop caused by the temperature gradient is the major driving force. In addition, as the fluid-wall interaction is strengthened, the flow flux assumes a maximum, where ε_{fw} is close to the lower temperature T_L of the channel and $\varepsilon_{fw}/kT_L \approx 1$ is roughly satisfied. © *2012 American Institute of Physics.* [http://dx.doi.org/10.1063/1.3693334]

I. INTRODUCTION

Fluid flows in micro- and nanochannels have tremendous applications in both science and engineering.[1–3] In small confinements, fluid transport can be very complex because it involves parameters at different scales, which are usually coupled with each other.[4] In the nanoscale, solid surfaces play important roles in understanding fluid motions due to the high surface area to volume ratio. A solid surface may cause fluctuations in fluid properties, such as density and viscosity. It may also bring about fluid adsorption and lead to different phenomena.[4–8] Therefore, surface properties or fluid-surface interactions impose major challenges to nanofluidics. In nanoscale flow systems, surface effects can greatly affect the transport of fluids, which is an important issue for the miniaturization of fluidic systems.[9–13]

In the past decade, different pumping methods have been developed to drive fluids in nanochannels. In these approaches, an external force is generated using mechanical, electrostatic or acoustic principles to pump the fluid.[14–23] These techniques may provide efficient ways to transport fluids in nanochannels for various applications, such as nanoparticle sorting, biomolecule separation, and chemical analysis.[1,3,24] Recently, we studied nanochannel flows and found that the coupling of temperature and surface effects could lead to different flow fashions.[4,25] We have numerically demonstrated that a fluid can be continuously circulated by a symmetric temperature gradient in nanochannels of heterogeneous surface energies. This fluid transport mechanism can be employed for thermal management by using the waste heat generated by chips/devices instead of external forces. However, the mechanism of fluid transport caused by temperature gradients in single material nanochannels (uniform surface energy) is not well understood and requires intensive investigations before it is used for practical applications.

In this work, we study the fluid transport induced by temperature gradients in nanochannels of uniform material through molecular dynamics (MD) simulations. In low surface energy channels (weak fluid-wall interaction), the fluid moves from high to low temperature and the flow is induced by a potential ratchet near the channel surface. In high surface energy channels, however, the fluid transports from low to high temperature and the flow is generated by the pressure difference due to the reorganization of the fluid triggered by the strong fluid-wall interaction. Furthermore, in high surface energy channels, it is found that the flow flux assumes a maximum when the fluid-wall binding energy is comparable to the lower temperature of the wall.

II. MOLECULAR DYNAMICS SIMULATION

A typical MD simulation system is shown in Fig. 1. It consists of two parallel solid walls with a fluid confined in between. The fluid is in connection with two reservoirs at the ends of the system. The walls are generated by cutting four layers of atoms from a face-centered cubic structure with lattice constant equal to 4.086 Å. To make the simulation system stable while considering the thermal motion of the wall, the atoms in the outmost layers of the walls are secured whereas the other wall atoms are free to vibrate under intermolecular interactions. The planner walls are perpendicular to the y axis. The lengths of the simulation system are 16 and 5 nm in the x and z directions, respectively. The channel width, D, distance between the innermost atomic layers of the walls, is 2 nm and the length is 8 nm (for 2 nm channels, simulations show that the length of the reservoirs should be larger than 2 nm to reduce the size effect of the reservoirs).

The channel wall is described by the tight-binding potential and the parameters for Ag are used.[4] The tight-binding potential is quite different from the simple spring-mass model. It has been widely used for transition metals and is good for considering the thermal motion of atoms and
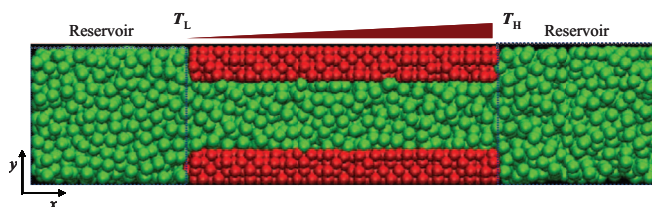
a)Electronic mail: mezli@ust.hk.

FIG. 1. Schematic of the simulation system. The green and red particles are the fluid molecules and wall atoms, respectively. The fluid in the channel is connected to two reservoirs at the ends of the system. A temperature gradient is applied along the wall by maintaining the temperature at the right end higher than that at the left end.

energy accommodation of solids. The interaction of the fluid molecules is modeled by the Lennard-Jones (LJ) 12-6 potential, $U(r) = 4\varepsilon_{ff}[(\sigma_{ff}/r)^{12} - (\sigma_{ff}/r)^6]$, where r is the distance between a pair of interacting molecules, ε_{ff} is the fluid-fluid binding energy, and σ_{ff} is the collision diameter of the fluid molecules. The interaction parameters, $\varepsilon_{ff} = 9.8 \times 10^{-3}$ eV and $\sigma_{ff} = 3.47$ Å, for liquid Ar are used. The number density of the fluid is $\rho = 15.38$ nm^{-3}. The interaction between fluid molecules and wall atoms is also calculated by the LJ potential and the fluid-wall binding energy ε_{fw} and collision diameter σ_{fw} are obtained by using the Lorentz–Berthelot mixing rule based on the LJ potential parameters given in Refs. 26 and 27. To understand the surface effect on the flow, the fluid-wall binding energy ε_{fw} is arbitrarily varied. The potentials are truncated at 10.21 Å and Newton's equations are integrated with Beeman's leapfrog algorithm,[9] with time step equal to 1 fs. For the channel, periodic boundary conditions (PBCs) are employed in the x and z directions only. For the reservoirs, PBCs are used in all the directions and that in the x direction makes the pressure in the two reservoirs the same. A temperature gradient is applied to the wall by maintaining constant temperatures at the ends of the wall. The temperature at the right end T_H is higher than that at the left end T_L of the channel. T_H and T_L are maintained at desired values by controlling the kinetic energy of the wall atoms in a slit of 5 Å near the ends of the wall through Berendsen thermostats,[28] which are also used to keep the temperature of the fluid in the reservoirs at 300 K. The simulation systems are relaxed for 2 ns before the flow properties are calculated.

III. RESULTS AND DISCUSSION

By fixing the low temperature T_L at 300 K and varying the high temperature T_H from 400 to 600 K, we compute the volumetric flux Q of the fluid under different surface conditions. Figure 2 plots the flux as a function of the fluid-wall binding energy ε_{fw}. It is seen that Q changes from negative to positive as ε_{fw} is increased. In low surface energy channels, the fluid moves from high to low temperature. If the surface energy of the channel is relatively high, however, the fluid is driven from low to high temperature. Figure 3 depicts the velocity profiles for a strong ($\varepsilon_{fw} = 300$ K) and a weak ($\varepsilon_{fw} = 10$ K) fluid-wall interaction case with $T_H = 500$ K. In Fig. 3(a), it is seen that the velocity distribution is quite uniform across the channel for the strong ε_{fw} case. For
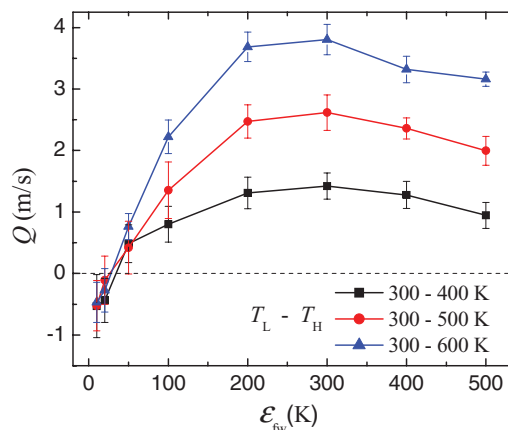

FIG. 2. The volumetric flux Q of the fluid as a function of fluid-wall binding energy ε_{fw} under different temperature gradients.

the weak ε_{fw} case [Fig. 3(b)], however, the velocity profile seems to be parabolic and the flow near the wall moves faster than in the center region. The slip length in Fig. 3(b) is roughly 0.84 nm if it is calculated as the ratio of the velocity to velocity gradient at the wall,[29] which is smaller than that in shear flows.[30] Due to the fact that the temperature variation along the channel affects the velocity profile (see Ref. 4), the velocity profiles in Fig. 3 are the average along the channel.
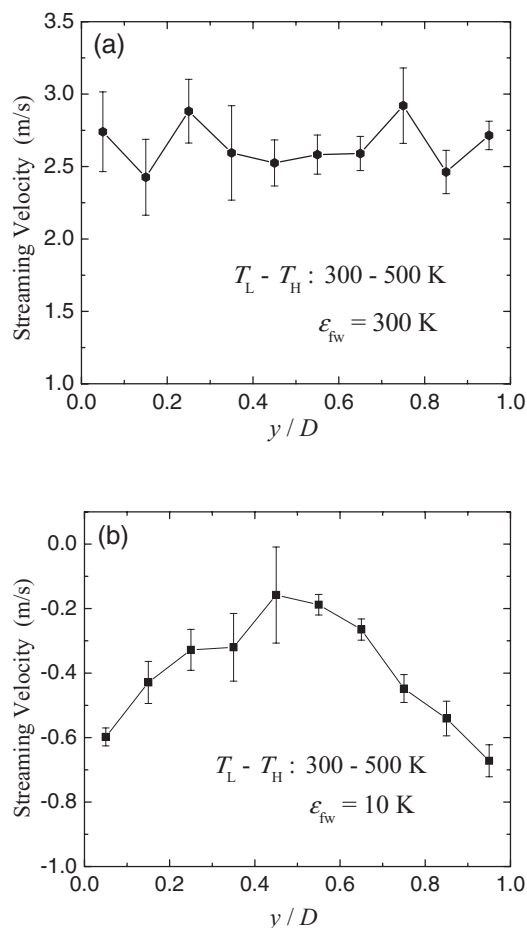

FIG. 3. The velocity profiles of the fluid with $T_L = 300$ and $T_H = 500$ K. (a) $\varepsilon_{fw} = 300$ K and (b) $\varepsilon_{fw} = 10$ K.
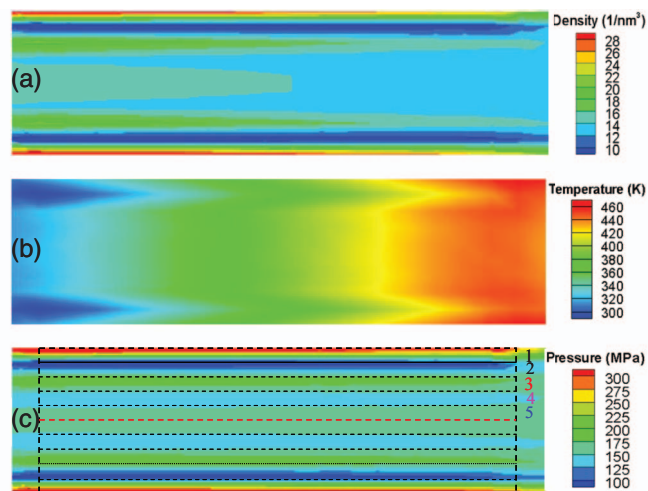
FIG. 4. Two-dimensional contour plots of density (a), temperature (b), and pressure (c) of the fluid in the channel for the case in Fig. 3(a) ($T_L = 300$, $T_H = 500$ K, and $\varepsilon_{fw} = 300$ K).

The distinct velocity distributions in the two cases indicate that the surface properties are coupled with temperature gradients and the flow mechanisms might be different.

To understand the flow phenomena, we investigate the flow properties in the channel. In nanochannels, the density distribution of fluids is usually non-uniform due to the wall effects,[4,7–12] which will lead to pressure variation. In addition, the temperature gradient in the wall will also affect the pressure. The pressure P of the fluid can be calculated using the virial equation of state[28]

$$P = \rho kT + \sum_i \sum_{j>i} r_{ij} F_{ij}/3\forall, \qquad (1)$$

where ρ is the fluid number density, k is the Boltzmann constant, F is the force between a pair of interacting molecules, and $\forall$ is the volume. The two terms in Eq. (1) represent the kinetic and potential components of the pressure, respectively. Given the molecular interaction, the kinetic component depends on both density and temperature, while the potential part is only determined by the density. The contributions of the two components to the pressure can be different, depending on the coupling of temperature and surface effects. Figure 4 shows the two-dimensional contour plots of fluid density, temperature, and pressure for the case of Fig. 3(a). In Fig. 4(a), it is seen that the density fluctuates greatly in the direction perpendicular to the wall plane and several molecular layers are observed near the walls. There are low density regions between two adjacent molecular layers, where the potential is less favorable for fluid molecules to stay. The formation of the clear molecular layers is caused by the strong fluid-wall interaction.[4,5,7–12] Furthermore, the temperature gradient in the channel [Fig. 4(b)] also generates density variation in the x direction. Because fluid adsorption is favored at low temperature, the highest density takes place at the low temperature end near the wall. The pressure distribution in Fig. 4(c) also fluctuates, especially in the y direction.

To show the pressure change in the flow direction, the fluid domain is partitioned into several bins parallel to the walls, as shown in Fig. 4(c). The pressure variations in the x direction in these bins are shown in Fig. 5(a). It is seen that the pressure decreases with increasing x or temperature T in bins 1, 3, and 5, which is similar to the density variation in these bins [Fig. 5(b)]. This indicates, based on Eq. (1), that the contribution of the potential component to the pressure dominates over the kinetic component in these bins. In bins 2 and 4, where the fluid density is low and the
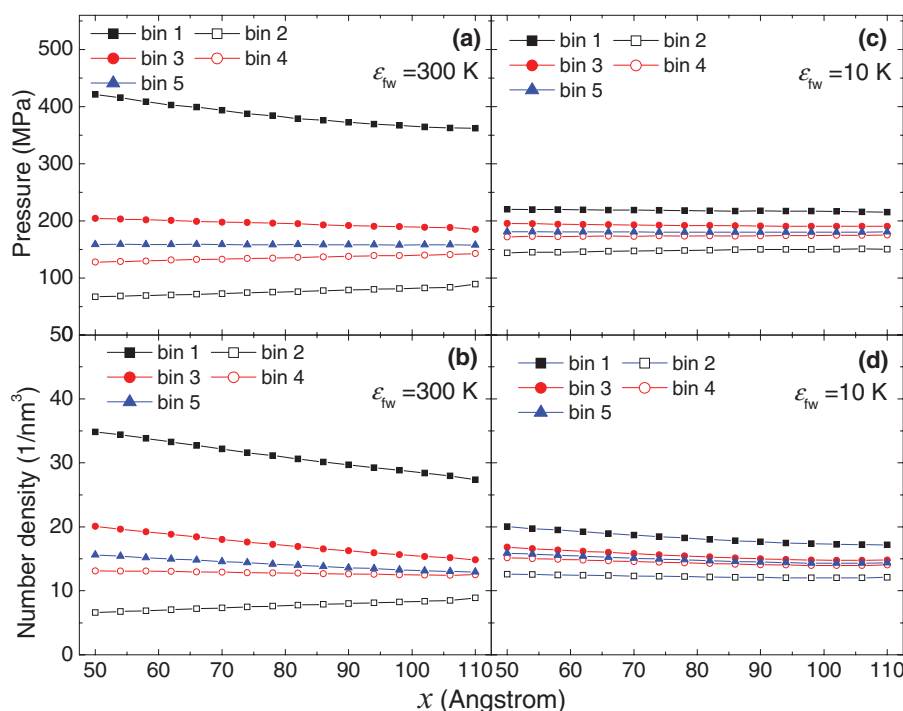

FIG. 5. The pressure and density distributions in the bins given in Fig. 4(c) for $T_L = 300$ and $T_H = 500$ K. $\varepsilon_{fw} = 300$ K in (a) and (b); $\varepsilon_{fw} = 10$ K in (c) and (d).

kinetic component becomes important, the pressure increases slightly as x increases. The density in bin 5 represents that in the center of the channel, which changes from 15.6 to 12.9 nm^{-3} with the average equal to 14.14 nm^{-3}. However, the pressure changes in high density bins are the major reason for generating the flow. Therefore, the flow transport from low to high temperature in high surface energy channels is caused by the pressure drop along the channel due to the density variation.

By following the same approach, the density and pressure distributions are also examined in low surface energy channels. Figures 5(c) and 5(d) show the pressure and density variations for the case of Fig. 3(b) ($\varepsilon_{\text{fw}} = 10$ K). It is observed that the density in all the bins decreases with increasing temperature. In low surface energy channels, the fluid-wall interaction is weak and the surface effect is insignificant. In this case, the temperature becomes a dominant factor. At high temperatures, the fluid molecules have strong thermal motion and therefore each molecule, on the average, takes more space due to the intermolecular interaction. This is why the density at high temperature end is lower than that at low temperature. For the pressure change, the kinetic component in Eq. (1) is supposed to dominate over the potential part considering that the density fluctuation in this case is smaller than the case of large ε_{fw}. However, the density change counteracts with the temperature gradient and the pressure variation due to the kinetic contribution is small. This explains why the pressure variation is unobservable along the channel, as shown in Fig. 5(c). Therefore, the pressure drop is not the driving force for the flow in low surface energy channels.

The parabolic velocity distribution with high speed near the wall in Fig. 3(b) indicates that the flow in low surface energy channels might be surface driven. If so, the fluid-wall intermolecular potential should play important roles. Figure 6(a) shows the potential distribution in the x-z plane 2.2 Å from the wall and Fig. 6(b) plots the cross-sectional view of the potential at $z = 0$ plane. It is clear that there exists a potential ratchet, which has a gradient in the energy barriers in the flow direction. The ratchet is generated by the atomic structure of the wall. The increasing magnitude of the ratchet in the positive x direction is the consequence of the thermal motion of the wall atoms due to the temperature gradient in the wall. When fluid molecules are close to the wall, they prefer to stay in the potential wells. After obtaining sufficient energy during the interactions with wall atoms, they prefer to move to the left because the energy barrier at low temperature is lower than that at high temperature. Therefore, the potential ratchet drives the fluid near the wall from high to low temperature.

Alternatively, the pumping effect in low surface energy channels can be explained by the interactions between the moving fluid molecules and vibrating wall atoms. For a fluid molecule moving toward the wall, it will "feel" the wall atoms at high temperature first because the thermal motion of these wall atoms is strong and their vibrational amplitude is large. Figure 6(c) shows the vibrational amplitude λ of the atoms in the innermost layer of the wall. λ_x and λ_y are obtained by averaging the maximum displacement from the equilibrium position in the x and y directions, as illustrated in the upper inset
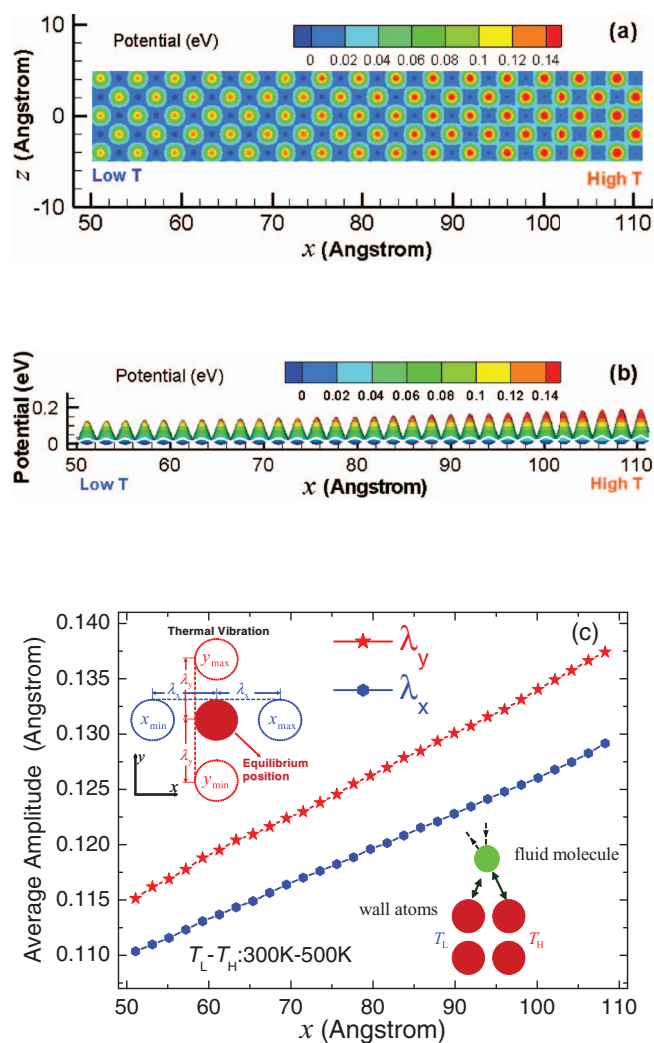

FIG. 6. (a) Two-dimensional contour plot of the potential in the x-z plane 2.2 Å to the wall with $T_L = 300$ and $T_H = 500$ K. (b) The cross-sectional view of the potential in $z = 0$ plane. (c) Average vibrational amplitude of wall atoms in the innermost layers. The definitions of λ_x and λ_y are depicted in the upper inset.

of Fig. 6(c). It is seen that λ_x and λ_y increase with increasing temperature. The gradient of λ causes force imbalance when the fluid molecule interacts with the wall atoms. As the fluid molecules approaches the wall, the repulsive force from the wall atoms at high temperature will push the molecule to the left [lower inset of Fig. 6(c)].

In Fig. 2, as the fluid-wall binding energy ε_{fw} is further increased, the flux assumes a maximum at $\varepsilon_{\text{fw}} \approx 300$ K, which is close to the low temperature T_L. Before the peak, as ε_{fw} increases, the wall effect becomes important and the density fluctuation in the fluid leads to large pressure drop, which enhances the flux, as discussed previously. When $\varepsilon_{\text{fw}} > 300$ K, $\varepsilon_{\text{fw}}/kT_L > 1$ and fluid adsorption tends to take place, starting from the low temperature end. Fluid adsorption will reduce the effective channel size and hinder the fluid motion. To confirm this, we conducted simulations by lowering the temperatures at the ends of the channel while keeping the same temperature gradient. Figure 7(a) shows the flux as a function of ε_{fw} for $T_L = 100$ and $T_H = 300$ K. It is seen that as T_L is reduced from 300 to 100 K, the binding energy for the
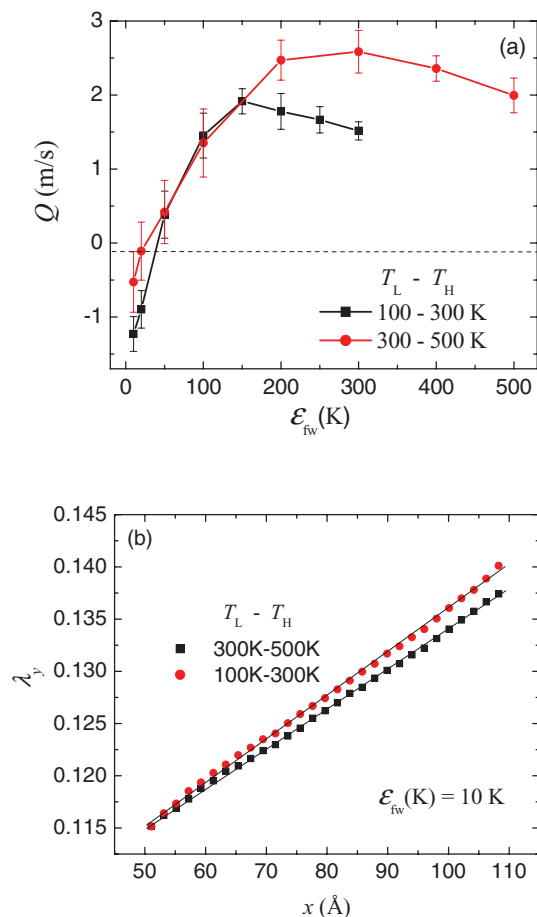
FIG. 7. The volumetric flux of the fluid versus ε_{fw} (a) and average vibrational amplitude of wall atoms (b) under different average temperatures. In (b), the data for $T_L = 100$ and $T_H = 300$ K are shifted up for clarity and the solid lines are the liner fit to the data.

maximum flux shifts to a lower value and $\varepsilon_{fw}/kT_L \approx 1$ is roughly satisfied. In addition, Fig. 7(a) also shows that a low temperature can enhance the pumping effect in the negative direction when ε_{fw} is small. This is because the gradient in the vibrational amplitude λ of the wall atoms in this case is larger than that in Fig. 6, as depicted in Fig. 7(b).

IV. SUMMARY

In summary, we have investigated the fluid transport in nanochannels induced by temperature gradients. As the fluid-wall binding energy is increased, the flow direction switches.

In channels of very low surface energy, the fluid moves from high to low temperature and the flow is driven by the potential ratchet near the wall. However, the fluid transports from low to high temperature in relatively high surface energy channels, where the flow is caused by the pressure drop along the channel due to the coupling of surface effect and temperature gradient. When the surface energy is increased further, the flux reaches the maximum, after which the fluid adsorption takes place and reduces the flow rate. The fluid-wall binding energy at the maximum flux roughly satisfies $\varepsilon_{fw}/kT_L \approx 1$.

[1]T. M. Squires and S. R. Quake, Rev. Mod. Phys. **77**, 977 (2005).
[2]P. A. Thompson and S. M. Troian, Nature (London) **389**, 360 (1997).
[3]S. Ghosh, A. K. Sood, and N. Kumar, Science **299**, 1042 (2003).
[4]C. Liu and Z. Li, Phys. Rev. E **80**, 036302 (2009).
[5]Z. Li and H. Wang, Phys. Rev. Lett. **95**, 014502 (2005).
[6]Z. Li and L. Hong, J. Chem. Phys. **127**, 074706 (2007).
[7]U. Heinbuch and J. Fischer, Phys. Rev. A **40**, 1144 (1989).
[8]M. Cieplak, J. Koplik, and J. R. Banavar, Phys. Rev. Lett. **86**, 803 (2001).
[9]Z. Li, Phys. Rev. E **79**, 026312 (2009).
[10]C. Liu and Z. Li, AIP Adv. **1**, 032108 (2011).
[11]C. Liu and Z. Li, J. Chem. Phys. **132**, 024507 (2010).
[12]N. V. Priezjev, A. A. Darhuber, and S. M. Troian, Phys. Rev. E **71**, 041608 (2005).
[13]A. Martini, H. Hsu, N. A. Patankar, and S. Lichter, Phys. Rev. Lett. **100**, 206001 (2008).
[14]S. Pennathur and J. G. Santiago, Anal. Chem. **77**, 6772 (2005).
[15]M. Rauscher, S. Dietrich, and J. Koplik, Phys. Rev. Lett. **98**, 224504 (2007).
[16]Z. Guttenberg, A. Rathgeber, S. Keller, J. O. Rädler, A. Wixforth, M. Kostur, M. Schindler, and P. Talkner, Phys. Rev. E **70**, 056311 (2004).
[17]J. L. Rivera and F. W. Starr, J. Phys. Chem. C **114**, 3737 (2010).
[18]Z. Insepov, D. Wolf, and A. Hassanein, Nano Lett. **6**, 1893 (2006).
[19]M. A. Soare, R. C. Picu, J. Tichy, T. M. Lu, and G. C. Wang, J. Intell. Mater. Syst. Struct. **17**, 231 (2006).
[20]A. Lohrasebi and Y. Jamali, J. Mol. Graphics Modell. **29**, 1025 (2011).
[21]Y. Wang, Y. J. Zhao, and J. P. Huang, J. Phys. Chem. B **115**, 13275 (2011).
[22]X. W. Meng, Y. Wang, Y. J. Zhao, and J. P. Huang, J. Phys. Chem. B **115**, 4768 (2011).
[23]H. Qiu, R. Shen, and W. Guo, Nano Res. **4**, 284 (2011).
[24]Z. Li and G. Drazer, Phys. Rev. Lett. **98**, 050602 (2007).
[25]C. Liu and Z. Li, Phys. Rev. Lett. **105**, 174501 (2010).
[26]P. M. Agrawal, B. M. Rice, and D. L. Thompson, Surf. Sci. **515**, 21 (2002).
[27]H. Hippler, J. Troe, and H. J. Wendelken, J. Chem. Phys. **78**, 6709 (1983).
[28]M. P. Allen and D. J. Tildesley, *Computer Simulation of Liquids* (Clarendon, Oxford England, 1989), p. 385.
[29]D. L. Morris, L. Hannon, and A. L. Garcia, Phys. Rev. A **46**, 5279 (1992).
[30]N. V. Priezjev, Phys. Rev. E **75**, 051605 (2007).